RSC Advances

ROYAL SOCIETY OF CHEMISTRY

www.rsc.org/advances

n-Type Small Aromatic Core Diimides Flanked With Electron Donating Thienylethyl Moiety and Electrical Responses in Organic Devices

Akshaya Kumar Palai[a#], *Sangwook Kim*[a#], *Hyunseok Shim*[a], *Sungwoo Cho*[b], *Amit Kumar*[a], *Jaehyuk Kwon*[a], *Seung-Un Park*[a], *Seungmoon Pyo*[a*]

[a]Department of Chemistry, Konkuk University, 120 Neungdong-ro, Gwangjin-gu, Seoul 143-701, Republic of Korea

[b]Center for Core Research Facility, Daegu Gyeongbuk Institute of Science & Technology, Daegu 711-873, Republic of Korea

Abstract

We report *n*-type small aromatic core diimide derivatives functionalized with electron donating heteroaromatic ring bearing moiety, *N*,*N*′-bis[2-(2-thienyl)ethyl]-benzene-1,2,4,5-tetracarboxylic diimide and *N*,*N*′-bis[2-(2-thienyl)ethyl]-napthalene-1,4,5,8-tetracarboxylic diimide. The synthesis, characterization of the newly synthesized diimides based organic semiconductors and electrical responses in electronic devices are investigated in detail. The structure, electrochemical and optical properties of the diimide derivatives were determined using ^{1}H NMR, ^{13}C NMR, mass spectrometry, UV-visible spectroscopy and cyclic voltammetry. The electron density distribution of the materials was also studied using density functional theory calculations to relate the structure and device's characteristics. The materials were employed for the preparation of organic thin-film transistors with inorganic and polymeric gate dielectrics at various substrate temperatures, and the device's electrical characteristics have been analyzed in detail. We also further explore its applicability in advanced electronic devices by fabricating a resistance load-type organic inverter, and the dynamic response behavior was investigated.

Keywords: Diimide, polymer gate dielectric, organic thin-film transistor, *n*-channel semiconductor

[#]Authors have equal contribution

[*]Corresponding author (pyosm@konkuk.ac.kr)

1. Introduction

Over the last few decades, organic thin-film transistors (OTFTs) have attracted widespread interest and huge progress has been achieved on their application in versatile electronic devices [1]. Accordingly, significant efforts have been targeted toward the development of a wide variety of organic/polymers for the ultimate goal of generating inexpensive organic devices [2]. In organic small-molecule-based TFTs, polycyclic aromatic compounds are preferentially used as the semiconducting materials [3]; e.g., acene derivatives [4] and diketopyrrolopyrrole (DPP) derivatives [5] as the *p*-channel components and fullerene derivatives [6] and rylene diimide derivatives [7] as the *n*-channel semiconductors. Recently, we demonstrated that easily accessible, small molecular DPPs could be used for *p*-channel OTFTs [8]. In contrast to *p*-channel small molecules, where a large variety of chemical structures have been presented, there remains a need to explore easily derivable, inexpensive small molecule-based *n*-channel semiconductors.

Rylene diimide derivatives are well-known aromatic electron-transport materials that are used in a variety of organic electronic devices because of their excellent thermal and environmental stability [9]. In particular, pyromellitic diimide (PMDI), naphthalene diimide (NDI) and perylene diimide (PDI) are the most extensively studied organic semiconductor (OSC) materials for *n*-channel OTFTs owing to their relatively high electron affinities and the versatile tunability of their optical and electrochemical properties via parent core extension or functionalization [10]. Unlike the core alteration, chemical structure engineering through a functionalization at the *N*-position of imide is a simple one-pot synthetic approach to a variety of aromatic derivatives for *n*-channel OTFTs [11]. The relatively facile synthesis of pyromellitic diimide (PMDI) and NDI derivatives in comparison to that of PDI derivatives enables more efficient large-scale production. Hence, a large number of *N*-functionalized PMDI and NDI derivatives with various side chains have been reported as a channel layer material for OTFTs [9a]. A series of NDI derivatives with alkylthienyl moieties have been reported and their spectroscopic, electrochemical, electronic, and structural properties were investigated in detail [12]. The Asha's group

also prepared a series of amide-functionalized NDIs for improved charge-carrier mobility, and described the effect of hydrogen bonding on the self-assembly of NDIs [13]. Lee *et al.* investigated two *n*-type soluble NDI derivatives with phenylmethyl and (trifluoromethyl)benzyl groups in the *N*-position of NDI [14]. An alkylphenyl functionalized NDI [15] and a 2-phenylethyl functionalized PDI derivative (BPE-PTCDI) [16] for a high performance *n*-channel OTFTs have been reported by Katz's and Bao's group, respectively. It is also reported that the aromatic/heteroaromatic ring bearing side chains in the rylene diimide derivatives have a potential role in controlling molecular packing and optoelectronic properties [17].

Here, we report the synthesis and characteristics of new small aromatic core diimide derivatives which have different core size and are functionalized with heteroaromatic ring (thienylethyl group) at the *N*-position of the core. We also report the static/dynamic characteristics of the aromatic core diimide derivatives based organic electronic devices with inorganic/organic dielectric fabricated at different substrate temperature.

2. Experimental

Details of the materials and instruments used in the synthesis and characterization are described in the Materials and Instruments section of the Supporting Information.

2.1 *Synthesis of N,N'-bis[2-(2-thienyl)ethyl]-benzene-1,2,4,5-tetracarboxylic diimide* (**3a**):

Benzene-1,2,4,5-tetracarboxylic dianhydride (500 mg, 2.29 mmol) was dissolved in dimethylformamide (DMF; 10 mL). 2-Thiophene ethylamine (640.8 mg, 5.04 mmol) was added and the resultant mixture was stirred at 110 ℃ overnight under a nitrogen atmosphere. After cooling to ambient temperature, the mixture was filtered and washed with methanol. A white flake like solid (920 mg) was obtained with a yield of 92%. The material was purified by vacuum sublimation. ^{1}H NMR ($CDCl_3$, 400 MHz): δ = 8.25 (s, 2H), 7.15 (m, 2H), 6.91 (d, 2H), 6.86 (d, 2H), 4.04 (t, 4H), 3.28 (t, 4H). ^{13}C ($CDCl_3$, 100 MHz): δ = 165.91, 139.39, 137.13, 127.08, 127.08, 125.83, 124.40, 118.37, 39.99, 28.31. Mp: 276.4

^{o}C.

2.2 ***Synthesis of N,N′-bis[2-(2-thienyl)ethyl]-naphthalene-1,4,5,8-tetracarboxylic diimide*** (**3b**):

1,4,5,8-Naphthalene-1,4,5,8-tetracarboxylic dianhydride (200 mg, 0.745 mmol) was dissolved in dimethylformamide (DMF; 6 mL). 2-Thiophene ethylamine (208.7 mg, 1.64 mmol) was added and the resultant mixture was stirred at 110 ℃ overnight under a nitrogen atmosphere. After cooling to ambient temperature, the mixture was filtered and washed with methanol. A yellowish brown solid (300 mg) was obtained with a yield of 83%. The material was purified by vacuum sublimation. Mp: 277.1 ^{o}C. ^{1}H NMR ($CDCl_3$, 400 MHz): δ = 8.76 (s, 4H), 7.14-6.92 (m, 6H), 4.48 (t, 4H), 3.29 (t, 4H). ^{13}C ($CDCl_3$, 100 MHz): δ = 162.67, 140.16, 131.08, 127.08, 127.01, 126.59, 125.71, 124.13, 42.05, 28.11. HRMS $[M+H]^+$, m/z calcd for $C_{26}H_{18}N_2O_4S_2$: 487.562, found: 487.3613.

2.3 ***Thin-film transistor fabrication and characterization***:

Three types of gate dielectric were used for the fabrication of OTFTs with the synthesized aromatic diimide small molecules: (i) *p*-doped Si/bare SiO_2 (300 nm) (capacitance (C_i) = 100 pF/mm^2), (ii) *p*-doped Si/OTS-treated SiO_2 (300 nm) (C_i = 110 pF/mm^2), and (iii) ITO/cross-linked poly(4-vinylphenol) (CL-PVP) (C_i = 61.04 pF/mm^2). A metal-insulator-metal (MIM, active area of 0.203 cm^2) device was used to measure the capacitance of the gate dielectrics. The Si/SiO_2 and glass/ITO substrates were cleaned as per a previously reported procedure [8]. An *n*-octadecyltrichlorosilane self-assembled monolayer was deposited over Si/SiO_2 by spin-coating (3000 rpm, 10 s) a 0.05 M OTS solution (in toluene) immediately after UV-ozone treatment; the OTS-treated substrate was then baked at 80 ℃ for 3 min. Using our previously reported method, a robust uniform thin-film of cross-linked poly(4-vinylphenol) (CL-PVP) on a glass/ITO substrate was obtained as a gate dielectric [18]. The active layer (50 nm) of **3a** or **3b** was deposited by thermal vacuum evaporation on top of the dielectrics at varied substrate temperatures (25, 45, and 60 ℃) at a fixed rate of 0.2 Å/s. Finally, gold source and drain electrodes (50 nm) were thermally deposited under high vacuum (6×10^{-6} Torr) at a rate of 0.3 Å/s. During Au deposition, a shadow mask was used to define the channel length (L) and width (W) of 50

and 1000 µm, respectively. An HP 4156A semiconductor analyzer was used to determine the electrical characteristics of the OTFTs under vacuum.

2.4 *Organic inverter fabrication and characterization*:

A resistive-load-type inverter was constructed by connecting the **3b** OTFT fabricated at T_s of 45 ^oC with the OTS-treated SiO_2 and an external resistive load (100 MΩ). To characterize the dynamic response of the transistor, a function generator (maximum 60 MHz; Rigol DG4062) was used to supply the input voltage. The output voltage response was detected using a digital oscilloscope (100 MHz; Rigol DS2102). A high-voltage amplifier (1 MHz, 400 Vp-p, Pintek HA-405) was used to amplify the signal and a Keithley 6517A was used as the power supply.

3. Results and discussion

The synthetic schematic of thienylethyl-functionalized pyrromelittic (**3a)** and naphthalene diimides (**3b)** are shown in Fig. 1. The materials were successfully prepared using an amine/DMF/110 ℃ protocol [19] with a high yield (92% for **3a** and 83% for **3b**). The chemical structures were identified by spectroscopic analysis (Supporting Information, Fig. S1-S2) and the corresponding data are provided in the experimental section.

DFT calculations [B3LYP/6-31G(d,p) level] of the energy levels using SPARTAN10 [20], predicted a LUMO energy level of -3.21 eV for **3a** and -3.47 eV for **3b** in vacuum and their respective HOMO energy levels are at -6.30 and -6.17 eV, respectively. Electron density distribution of the LUMO (a and b) and HOMO (c and d) of **3a** and **3b** is depicted in Fig. 2. It is found that the lowest unoccupied molecular orbital density is distributed mainly on the core of the molecule and the highest occupied molecular orbital density is localized on thiophene unit (side chain) suggesting that the core of the material is electron accepting in nature. Similar predominant localization of the LUMO and HOMO wave functions on the acceptor and donor units, respectively, has been reported for a set of rylene and related diimide derivatives [21, 22]. The LUMO energy of **3a** and **3b** was also experimentally calculated by cyclic voltammetry (Instrument section of the Supporting Information for details), as shown in inset

of Fig. 2 (right side) and Fig. S3a, respectively. The LUMO value of **3a** and **3b**, calculated by E_{LUMO} = -[4.8 - $E_{1/2,\ Fc/Fc+}$ + $E_{red,onset}$] eV [23], were found to be -3.29 and -3.91 eV, respectively. The onset potential of the first reduction wave of **3a** and **3b** are -1.13 and -0.51 V (**3b**), respectively, where $E_{1/2}$ of ferrocene is 0.38 V. The optical properties of **3a** and **3b** in chloroform were investigated via UV-visible spectroscopy and the corresponding absorption spectra are shown in Fig. S3. The absorption bands for **3a** are centered at 320 and 310 nm where as for **3b** the peaks are at 362 and 382 nm respectively. Optical bandgaps calculated from absorption cut off values are 3.65 and 3.05 eV for **3a** and **3b**, respectively. The thermal properties of the materials were investigated through a thermogravimetric analysis (TGA) and differential scanning calorimetry (DSC). The thermal decomposition temperatures with a 5% weight loss were calculated to be 328 ℃ and 395 ℃ for **3a** and **3b**, respectively (Fig. 3a). Differential scanning calorimetry (DSC) analysis revealed that the materials showed clear exothermic crystallization and endothermic melting temperature at 267 and 277.1 ℃ for **3b** (Fig. 3b) and at 273 and 276.4 ^{o}C for **3a**, respectively (inset, Fig. 3b). These results reveal that their thin-film could be easily prepared through a thermal vacuum evaporation over a broad range of substrate temperatures without any thermal degradation during the film formation.

The OTFTs based on **3b** show well-defined *n*-channel characteristics (discussed in the later part). On the other hand, the device based on **3a** showed no such characteristics. It is clearly different observation from other diimide derivatives with pyromellitic diimide core (**4a** and **4b,** Fig. 1) exhibiting *n*-channel transport behavior [19]. The reported diimides (**4a** and **4b**) have fluorinated side chain that stabilizes the LUMO energy level. However, in our pyromellitic diimide (**3a**), electron donating thienylethyl group is introduced as a side chain, resulting in the higher LUMO energy level. The higher LUMO level of **3a** may increase charge injection barrier (1.99 eV) from Au electrode (ϕ_m = 5.2 eV) [24], that is relatively higher than those of **4a** (1.74 eV) and **4b** (1.66 eV) (See the inset of Fig. 2). On the other hand, the **3b** with an extended diimide core shows lower lying LUMO energy compared to **3a**, and the devices based on **3b** showed good *n*-channel OTFT properties. It can be inferred from the above

reasons that the electrical characteristics of small aromatic core diimide derivatives could be affected by the core size and the type of introduced side group. The theoretically calculated LUMO energy levels of all the discussed materials are depicted in inset of Fig. 2 (left side). Based on the results, we further investigated in detail the performance of OTFTs with **3b** deposited on different gate dielectrics such as OTS-treated SiO_2, and cross-linked poly(4-vinylphenol) at various substrate temperature in order to explore its potential applicability as an organic semiconductor in advanced OTFTs.

It could be inferred from the device results (discussed in the later section) that the electron mobilities of the device are dependent on the type of gate dielectric and T_s [11b, 25, 26]. Atomic force microscopy (AFM) and X-ray diffraction (XRD) analysis were performed on the **3b** thin-film to understand the variation in the performance of the OTFTs with different gate dielectrics and T_s. Fig. 4(a-c) show the AFM height profiles of the **3b** thin-film deposited at a T_s of 45 ℃ onto bare SiO_2, OTS-treated SiO_2, and CL-PVP, respectively, while those on the various gate dielectrics at T_s of 25 and 60 ℃ are depicted in Fig. S5. The images reveal that the grain size increases slightly with increasing T_s but retains an almost identical crystal shape. Although there are many reports on the increased charge-carrier mobility with increasing grain size [16c, 19, 27], our initial studies showed the opposite trend; the mobility decreased with increasing grain size that are also observed by Park group [28]. It has been suggested by them that interconnection and improved contact between grains results in the enhancement of mobility, while the layer with larger voids could reduce the carrier mobility inspite of the formation of large grains. In our study we also observed larger grains of **3b** with bigger voids at higher T_s (60 ^{o}C) in the film may leads the decrease in the hole mobility. The AFM image of the **3b** thin-film on OTS-treated SiO_2 (Fig. 4b) prepared at T_s of 45 ℃ revealed improved contact between the grains with needle-like crystals, which were not observed on bare SiO_2 and CL-PVP. In addition, the device fabricated with OTS-treated SiO_2 at T_s of 45 ℃ showed the best device performance. This improvement in electron mobility may also be because of an increase in the crystallinity of the **3b** thin-film, which was evident from the XRD analyses. Fig. 4d shows the XRD patterns of the **3b** thin-films prepared at T_s of 45 ℃ on

bare SiO_2, OTS-treated SiO_2, and CL-PVP. The XRD patterns reveal that the **3b** on OTS-treated SiO_2 gives the highest diffraction intensity, which indicates improved crystallinity. Similar observations were reported by the Bao's group regarding BPE-PTCDI thin films on an OTS-treated SiO_2 [16c]. The XRD patterns of **3b** film (50 nm) on bare SiO_2, CL-PVP and OTS-treated SiO_2 substrates at various T_s are also depicted in Fig. S6. For all samples a diffraction peak at $2\theta = 6.47°$ was detected and the corresponding *d*-spacing was calculated to be 1.364 nm using Bragg's equation [$n\lambda = 2d \sin\theta$, where λ is the incident X-ray wavelength ($\lambda = 1.540598$ Å)].

We have investigated the characteristics of the OTFTs with **3b** (naphthalene diimide core) as channel layer material on bare SiO_2, OTS-treated SiO_2, and CL-PVP at different substrate temperatures (T_s) of 25, 45, and 60 ℃ and a representative bottom-gate, top-contact OTFT is shown in Fig. 5a. Fig. S4(a-c) show the representative output characteristics of the OTFTs prepared on bare SiO_2, OTS-treated SiO_2, and CL-PVP, respectively at T_s of 25 ℃. The output characteristic curves for all the devices clearly showed typical *n*-type characteristics. The transfer curves of all the devices fabricated with different gate dielectrics and T_s are shown in Fig. 5(b-d), and the device performance parameters are listed in Table 1. Fig. 5b shows the transfer characteristics of the OTFT fabricated on a bare SiO_2 at various T_s. The electron mobility extracted from the saturation regime were 6.2×10^{-4}, 5.5×10^{-4}, and 5.9×10^{-6} cm^2/Vs for the devices prepared at T_s of 25, 45, and 60 ℃, respectively. Similarly, OTFT devices based on an OTS-treated SiO_2 (Fig. 5c) at T_s of 25, 45, and 60 ℃, exhibited charge carrier motilities of 1.2×10^{-2}, 1.7×10^{-2}, and 3.8×10^{-3} cm^2/Vs, respectively. The OTFT devices with an OTS-treated SiO_2 showed much better performance with respect to charge-carrier mobility and I_{on}/I_{off} than that of devices with bare SiO_2. Devices with an OTS-treated SiO_2 exhibit I_{on}/I_{off} values in the range 10^4-10^5 and electron mobilities varying from 10^{-2} to 10^{-3} cm^2/Vs, which is almost 100 times higher than that of devices with a bare SiO_2. The enhanced performance may be caused by lower charge-carrier trap density at the interface between the gate dielectric and semiconducting channel. The effect of treatment of the SiO_2 surface with a self-assembled monolayer has been discussed in literature both for *p*-type [29]

and *n*-type semiconductors [16c, 30]. The highest mobility ~0.02 cm^2/Vs was achieved for the device fabricated at a substrate temperature of 45 ℃ on an OTS-treated SiO_2 gate dielectric. We also have analyzed devices with a polymer gate dielectric, poly(4-vinylphenol) (CL-PVP) (Fig. 5d) fabricated at T_s = 25, 45, and 60 ℃. The devices showed mobilities of 3.6×10^{-4}, 1.9×10^{-4}, and 7.6×10^{-5} cm^2/Vs, respectively, which are comparable or higher than those of bare SiO_2 devices. It indicates that the newly synthesized NDI derivative is potential active candidate for device with inorganic as well as organic gate dielectrics and flexible substrates.

To demonstrate the potential of the synthesized material for application in advanced organic electronics, load-type inverters were fabricated and characterized. The inverter, which is the fundamental logic element in an integrated circuit (IC) that converts low input (logic 0) to high output (logic 1) or vice versa, was constructed using a **3b** based OTFT fabricated at T_s of 45 ℃ with an OTS-treated SiO_2, the device exhibiting the best overall performance. A schematic diagram of the resistive-load inverter with an external resistive load (100 MΩ) is shown in Fig. 6a. We measured the dynamic response characteristics of the inverter at frequencies of 1 (Fig. S7a), 0.5 (Fig. 6b), and 0.1 Hz (Fig. S7b), with a fixed V_{DD} = 50 V. As shown in Fig. 6b, when a square wave of V_{IN} switching from 0 to 50 V at a fixed frequency, V_{OUT} exhibits a dynamic switching response to V_{IN} with a transient behavior just after the changes in the V_{IN} [31]. However, it does not generate square-like output waves because of a large overlap capacitance [32], which could be avoided by using a high dielectric insulator and/or designing an appropriate device structure. Similar dynamic behavior was reported by Lee et al. in a resistance load-type organic inverter [33].

4. Conclusions

In summary, we adopted the simplest one-pot synthetic procedure to obtain small aromatic core diimide molecules **3a** and **3b**. The best performance was observed from the **3b** device prepared using an OTS-treated SiO_2 substrate. The AFM images and XRD patterns reveal that the morphology and crystalline nature of the **3b** film varies according to the surface properties and substrate temperature during

deposition. The highest electron mobility of ~0.02 cm^2/Vs with an I_{on}/I_{off} of 3.14×10^4 was achieved for the **3b** TFT. We also demonstrated decent dynamic inverter action from our **3b**-TFT-based resistive load-type organic inverter. Moreover, the synthesized NDI derivative is compatible with polymer gate dielectric and hence could be used for advanced organic electronic device applications.

Appendix A. Supplementary material

Supplementary data associated with this article can be found in the online version.

Acknowledgments

This work was supported by the National Research Foundation (NRF) funded by the Korean government (MEST) (2012R1A2A2A01045694). A. K. P. acknowledges financial support from the 2012 KU Brain Pool Research Program of Konkuk University.

References

[1] (a) A. L. Briseno, *ACS Appl. Mater. Interfaces*, 2013, **5**, 2301;
(b) M. Magliulo, A. Mallardi , M.Y. Mulla, S. Cotrone , B. R. Pistillo, P. Favia, I. Vikholm-Lundin, G. Palazzo and L. Torsi, *Adv. Mater.*, 2013, **25**, 2090;
(c) H. Klauk, *Chem. Soc. Rev.*, 2010, **39**, 2643;
(d) C. D. Dimitrakopoulos and P. R. L. Malenfant, *Adv. Mater.*, 2002, **14**, 99.
[2] (a) J. Mei, Y. Diao, A. L. Appleton, L. Fang and Z. Bao, *J. Am. Chem. Soc.*, 2013, **135**, 6724;
(b) C. Wang, H. Dong, W. Hu, Y. Liu and D. Zhu, *Chem. Rev.*, 2012, **112**, 2208;
(c) A. Facchetti, *Chem. Mater.*, 2011, **23**, 733;
(d) T. Mori, *J. Phys.: Condens. Matter*, 2008, **20**, 184010.
[3] (a) W. Jiang, Y. Li and Z. Wang, *Chem. Soc. Rev.*, 2013, **42**, 6113.
(b) H. Glowatzki, P. Sonar, S. P. Singh, A. M. Mak, M. B. Sullivan, W. Chen, A. T. S. Wee and A. Dodabalapur, *J. Phys. Chem. C*, 2013, **117**, 11530.
(c) B. J. Jung, N. J. Tremblay, M.-L. Yeh, H. E. Katz, *Chem. Mater.*, 2011, **23**, 568;
(d) M. Stolar, T. Baumgartner, *Phys. Chem. Chem. Phys.*, 2013, **15**, 9007.
[4] (a) J. E. Anthony, *Chem. Rev.*, 2006, **106**, 5028;
(b) J. Park, L.-M. Do, J.-H. Bae, Y.-S. Jeong, C. Pearson, M. C. Petty, *Org. Electron.*, 2013, **14**, 2101;
(c) J. Takeya, M. Yamagishi, Y. Tominari, R. Hirahara, Y. Nakazawa, T. Nishikawa, T. Kawase, T. Shimoda and S. Ogawa, *Appl. Phys. Lett.*, 2007, **90**, 102120.
[5] (a) S. L. Suraru, U. Zschieschang, H. Klauk and F. Wurthner, *Chem. Commun.*, 2011, **47**, 1767;
(b) A. K. Palai, J. Lee, T. J. Shin, A. Kumar, S.-U. Park and S. Pyo, *Chem. Commun.*, 2014, DOI: 10.1039/c4cc02055c.
[6] (a) C. L. Chochos, N. Tagmatarchis and V. G. Gregoriou, *RSC Adv.*, 2013, **3**, 7160.
(b) T. D. Anthopoulos, B. Singh, N. Marjanovic, N. S. Sariciftci and A. M. Ramil, *Appl. Phys. Lett.*, 2006, **89**, 213504;
(c) M. Bendikov, F. Wudl and D. F. Perepichka, *Chem. Rev.*, 2004, **104**, 4891.
[7] (a) Q. Meng and W. Hu, *Phys. Chem. Chem. Phys.*, 2012, **14**, 14152;
(b) B. Mukherjee, K. Sim, T. J. Shin, J. Lee, M. Mukherjee, M. Ree and S. Pyo, *J. Mater.*

Chem., 2012, **22**, 3192;
(c) M. Mas-Torrent and C. Rovira, *Chem. Soc. Rev.*, 2008, **37**, 827.
[8] (a) A. K. Palai, H. Cho, S. Cho, T. J. Shin, S. Jang, S.-U. Park and S. Pyo, *Org. Electron.*, 2013, **14**, 1396;
(b) A. K. Palai, J. Lee, M. Jea, H. Na, T. J. Shin, S. Jang, S.-U. Park and S. Pyo, *J. Mater. Sci.*, 2014, **49**, 4215.
[9] (a) X. Zhan, A. Facchetti, S. Barlow, T. J. Marks, M. A. Ratner, M. R. Wasielewski and S. R. Marder, *Adv. Mater.*, 2011, **23**, 268;
(b) B. A. Jones, A. Facchetti, M. R. Wasielewski and T. J. Marks, *J. Am. Chem. Soc.*, 2007, **129**, 15259;
(c) R. Lygaitis, D. Gudeika, J. V. Grazulevicius and V. Jankauskas, *Synth. Met.*, 2013, **181**, 56;
(d) A. Pron, R. R. Reghu, R. Rybakiewicz, H. Cybulski, D. Djurado, J. V. Grazulevicius, M. Zagorska, I. Kulszewicz-Bajer and J.-M. Verilhac, *J. Phys. Chem. C*, 2011, **115**, 15008.
[10] (a) H. Luo, Z. Cai, L. Tan, Y. Guo, G. Yang, Z. Liu, G. Zhang, D. Zhang, W. Xu and Y. Liu, *J. Mater. Chem. C*, 2013, **1**, 2688;
(b) S.-L. Suraru, U. Zschieschang, H. Klauk and F. Wurthner, *Chem. Commun.*, 2011, **47**, 11504;
(c) L. Gisslen and R. Scholz, *Physical Rev. B*, 2011, **83**, 155311.
[11] (a) B. J. Jung, N. J. Tremblay, M.-L. Yeh and H. E. Katz, *Chem. Mater.*, 2011, **23**, 568;
(b) B. J. Jung, K. Lee, J. Sun, A. G. Andreou and H. E. Katz, *Adv. Funct. Mater.*, 2010, **20**, 2930.
[12] P. Gawrys, D. Boudinet, A. Kornet, D. Djurado, S. Pouget, J.-M. Verilhac, M. Zagorska and A. Pron, *J. Mater. Chem.*, 2010, **20**, 1913.
[13] N. B. Kolhe, R. N. Devi, S. P. Senanayak, B. Jancy, K. S. Narayan and S. K. Asha, *J. Mater. Chem.*, 2012, **22**, 15235.
[14] Y.-L. Lee, H.-L. Hsu, S.-Y. Chen and T.-R. Yew, *J. Phys. Chem. C*, 2008, **112**, 1694.
[15] (a) B. J. Jung, J. F. M. Hardigree, B. M. Dhar, T. J. Dawidczyk, J. Sun, K. C. See and H. E. Katz, *ACS Nano*, 2011, **5**, 2723;
(b) B. M. Dhar, G. S. Kini, G. Xia, B. J. Jung, N. Markovic and H. E. Katz, *PNAS*, 2010, **107**, 3972.
[16] (a) H. Yu, Z. Bao and J. H. Oh, *Adv. Funct. Mater.*, 2013, **23**, 629;
(b) J. H. Oh, H. W. Lee, S. Mannsfeld, R. M. Stoltenberg, E. Jung, Y. W. Jin, J. M. Kim, J.-B. Yoo and Z. Bao, *PNAS*, 2009, **106**, 6065;
(c) M.-M. Ling, P. Erk, M. Gomez, M. Koenemann, J. Locklin and Z. Bao, *Adv. Mater.*, 2007, **19**, 1123.
[17] G. Boobalan, P. M. Imran and S. Nagarajan, *ScienceJet*, 2013, **2:35**, 1-5.
[18] A. K. Palai, J. Lee, S. Das, J. Lee, H. Cho, S.-U. Park and S. Pyo, *Org. Electron.*, 2012, **13**, 2553.
[19] Q. Zheng, J. Huang, A. Sarjeant and H. E. Katz, *J. Am. Chem. Soc.*, 2008, **130**, 14410.
[20] *Spartan'10* Wavefunction, Inc. Irvine, CA
[21] Y. A. Getmanenko, L. E. Polander, D. K. Hwang, S. P. Tiwari, E. Galan, B. M. Seifried, B. Sandhu, S. Barlow, T. Timofeeva, B. Kippelen and S. R. Marder, *Journal of Organic Semiconductors*, 2013, **1**, 7.
[22] X. Chen, J. Wang, G. Zhang, Z. Liu, W. Xu and D. Zhang, *New J. Chem.*, 2013, **37**, 1720.
[23] P. Deng, L. Liu, S. Ren, H. Li and Q. Zhang, *Chem. Commun.*, 2012,**48**, 6960.
[24] (a) T. W. Hickmott, *J. Appl. Phys.*, 2010, **107**, 093714;
(b) Z. He, C. Zhong, S. Su, M. Xu, H. Wu and Y. Cao, DOI:10.1038/NPHOTON.2012.190.
[25] G. Generali, F. Dinelli, R. Capelli, S. Toffanin, F. D. Maria, M. Gazzano, G. Barbarella and M. Muccini, *J. Phys. Chem. C*, 2011, **115**, 23164.
[26] (a) D. Shukla, T. R. Welter, D. R. Robello, D. J. Giesen, J. R. Lenhard, W. G. Ahearn, D. M. Meyer and M. Rajeswaran, *J. Phys. Chem. C*, 2009, **113**, 14482.
(b) J. H. Lee, S. H. Kim, G. H. Kim, S. C. Lim, H. Lee, J. Jang, T. Zyung, *Synth. Metals*, 2003, **139**, 445;
(c) J.-I. Nishide, Y. Nakagawa and H. Sasabe, *Mol. Cryst. Liq. Cryst.*, 2009, **505**, 19/257.

[27] J. H. Oh, S. Liu, Z. Bao, R. Schmidt and F. Würthner, *Appl. Phys. Lett.*, 2007, **91**, 212107.
[28] S. Y. Yang, K. Shin, C. E. Park, *Adv. Mater.*, 2005, **15**, 1806.
[29] S. P. Tiwari, K. A. Knauer, A. Dindar and B. Kippelen, *Org. Electron.*, 2012, **13**, 18.
[30] R. Centore, L. Ricciotti, A. Carella, A. Roviello, M. Causa, M. Barra, F. Ciccullo and A. Cassinese, *Org. Electron.*, 2012, **13**, 2083.
[31] T. Fujimoto, Y. Miyoshi, M. M. Matsushita and K. Awaga, *Chem. Commun.*, 2011, **47**, 5837.
[32] M. Fadlallah, W. Benzarti and G. Billiot, *J. Appl. Phys.*, 2006, **99**, 104504.
[33] K. H. Lee, J.-M. Choi, S. Im, B. H. Lee and K. K. Im, *J. Appl. Phys.*, 2007, **91**, 123502.

Legends to Figures

Table 1. Summary of performance of OTFTs with **3b**

Figure 1. Synthesis scheme of new small core aromatic diimides. The structure of **4a** and **4b** are taken from reference no. 19.

Figure 2. Electron density distribution in (a, b) LUMO and (c, d) HOMO of **3a** and **3b,** respectively. Left inset: the energy level diagram of synthesized material compared with reported diimides. *These are taken from reference no. 19. Right inset: the CV curve of **3b** in DCM (scan rate: 50 mV s^{-1}).

Figure 3. (a) Thermogravimetric analysis (TGA) of synthesized materials and (b) Differential scanning calorimetry (DSC) curve of **3a** and **3b** in nitrogen with a heating and scanning rate of 10 ^{o}C/min, respectively.

Figure 4. Tapping-mode atomic force microscopy (AFM) images of **3b** thin-film (50 nm) on (a) bare SiO_2, (b) OTS treated SiO_2 and (c) CL-PVP at T_s = 45 ^{o}C. (d) Corresponding out-of-plane XRD patterns at the same substrate temperature.

Figure 5. (a) Schematic diagram of bottom gate, top-contact OTFT devices. Transfer characteristics of OTFTs with **3b** at different substrate temperature (T_s) (V_{DS} = 80 V) on various gate dielectrics: (b) bare SiO_2, (c) OTS-treated SiO_2 and (d) cross-linked polymer gate dielectric (CL-PVP).

Figure 6. (a) Schematic diagram of resistance-load type inverter based on **3b** OTFT (OTS treated SiO_2 substrate, T_s = 45 ^{o}C), (b) Dynamic behavior of the corresponding device operated under a supply voltage V_{DD} = 50 V, resistor R =100 MΩ and input voltage pulse = 0.5 Hz.

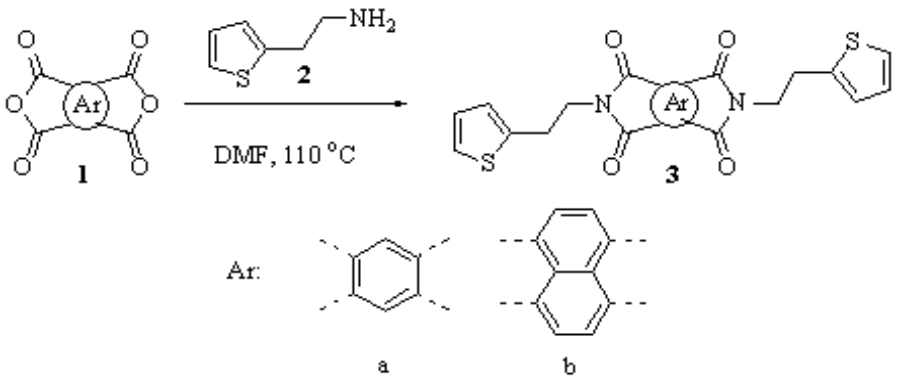

Scheme 1. Synthesis scheme of new small core aromatic diimides

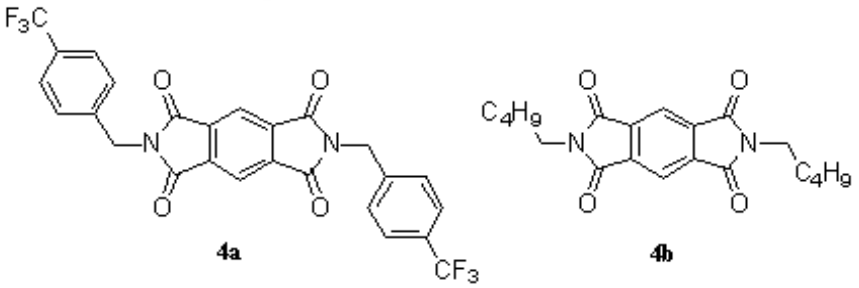

Figure 1

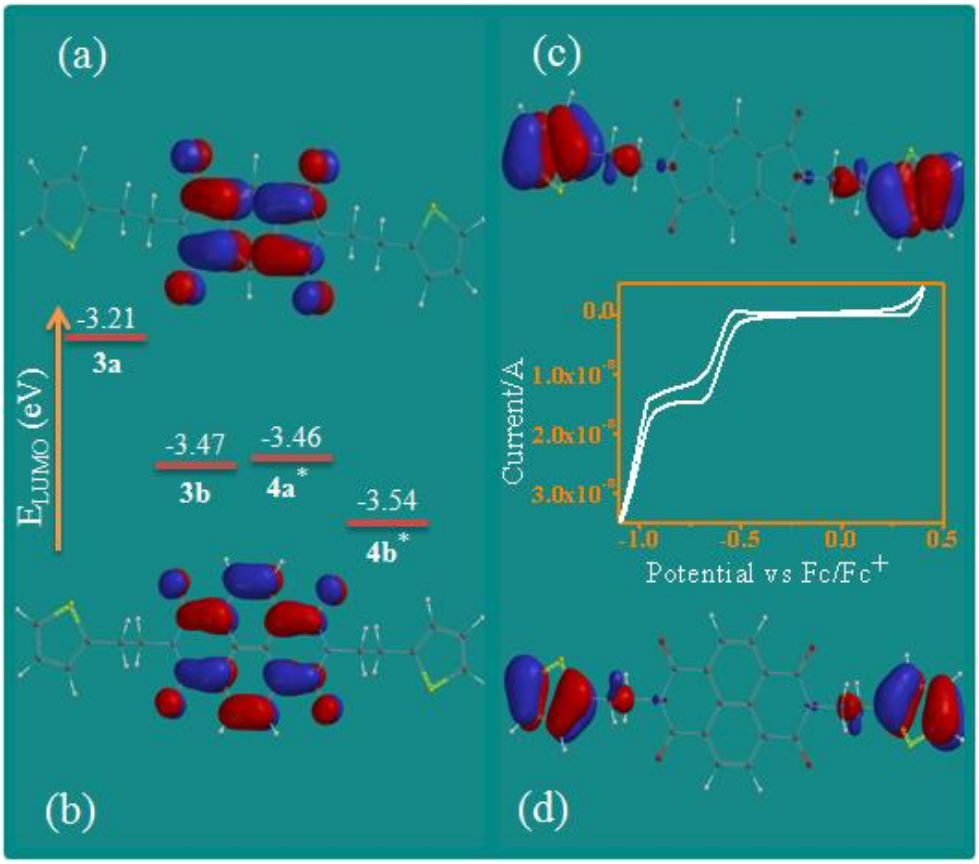

Figure 2

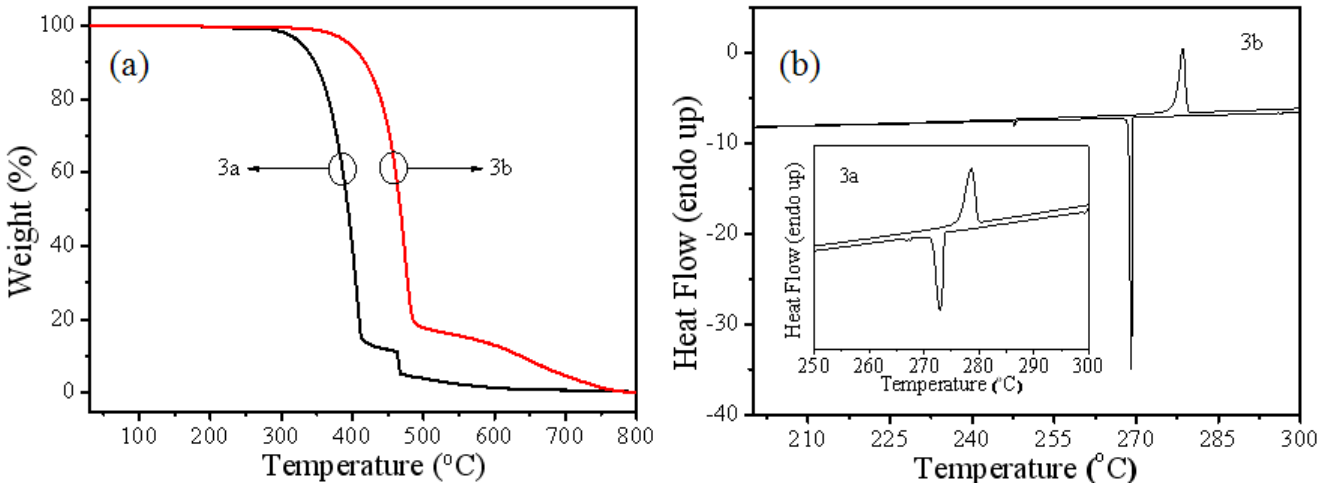

Figure 3

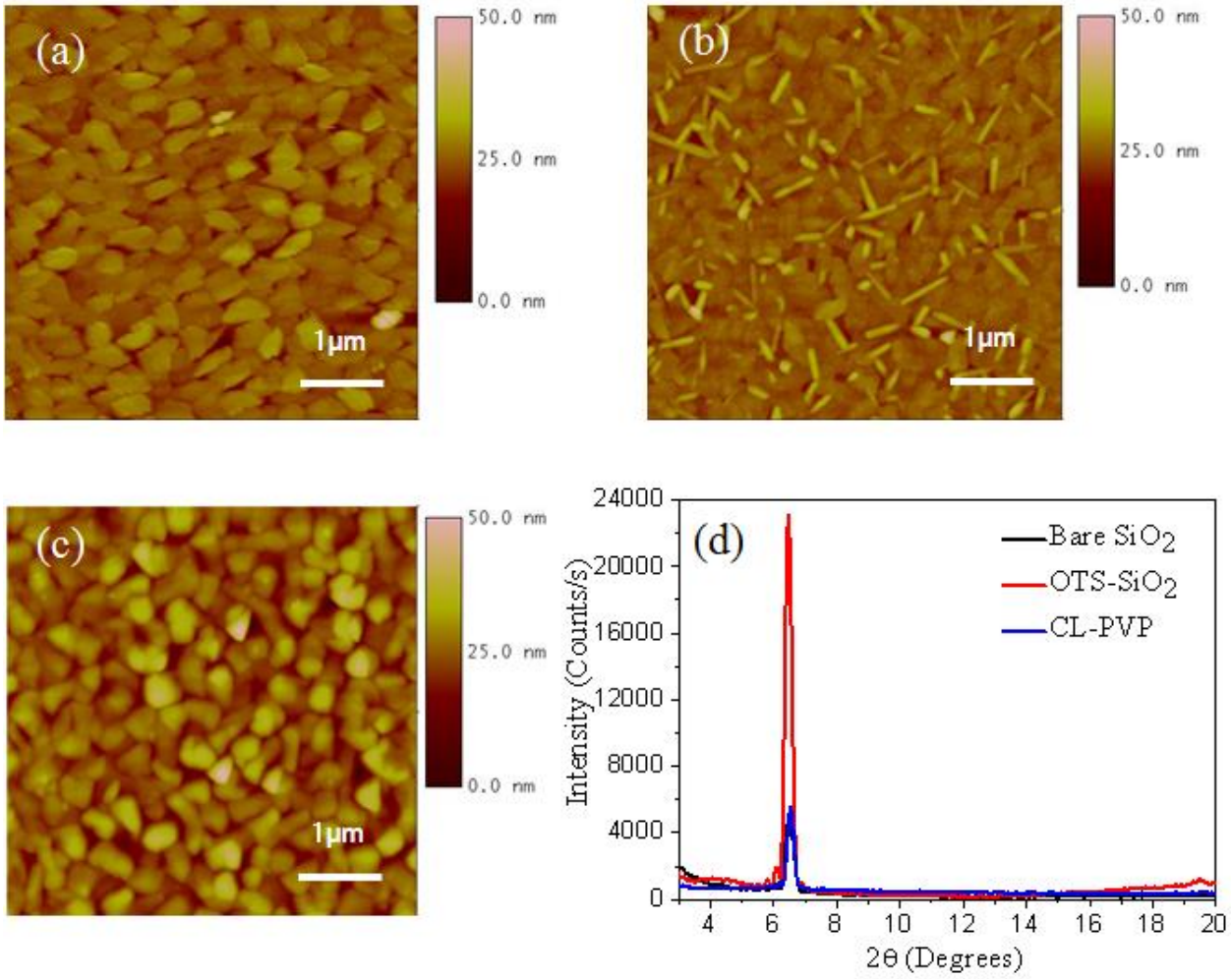

Figure 4

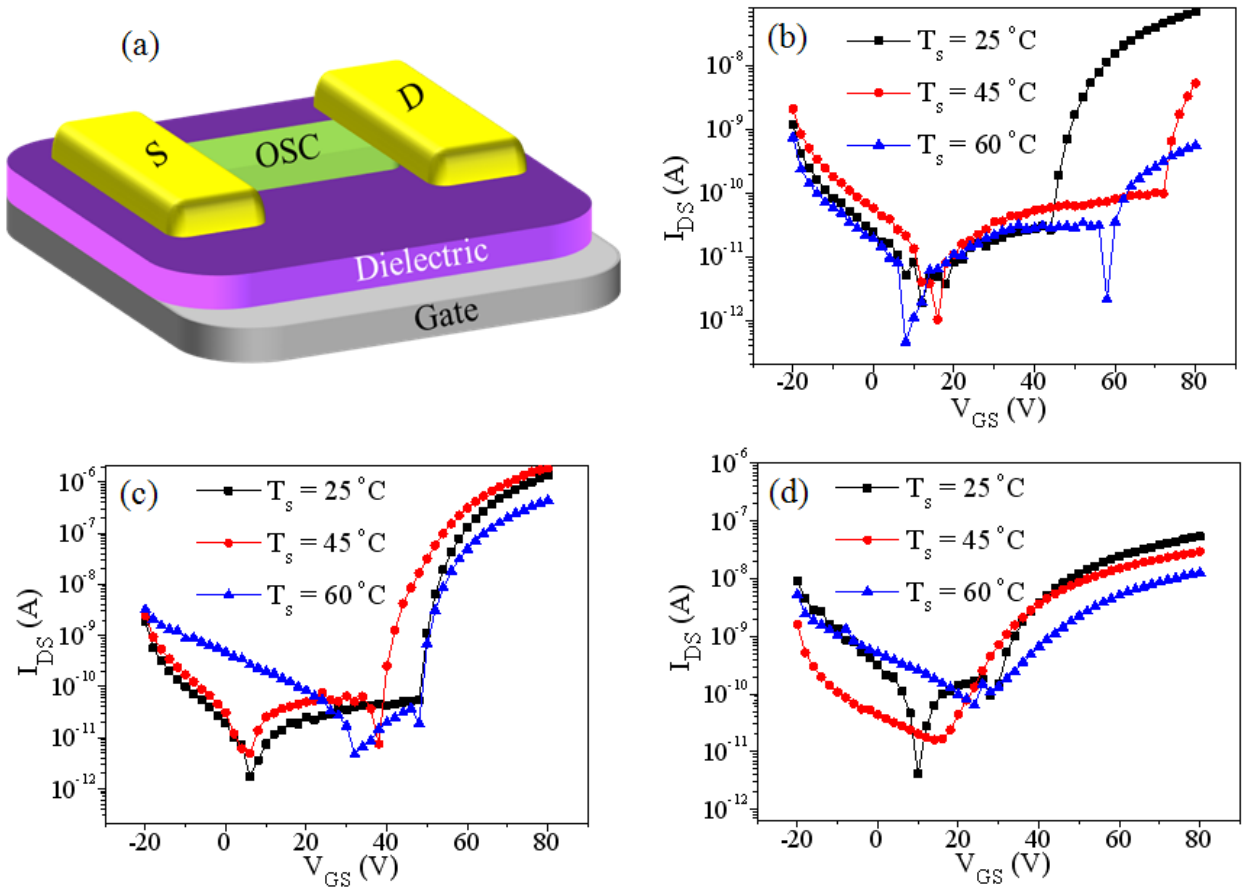

Figure 5

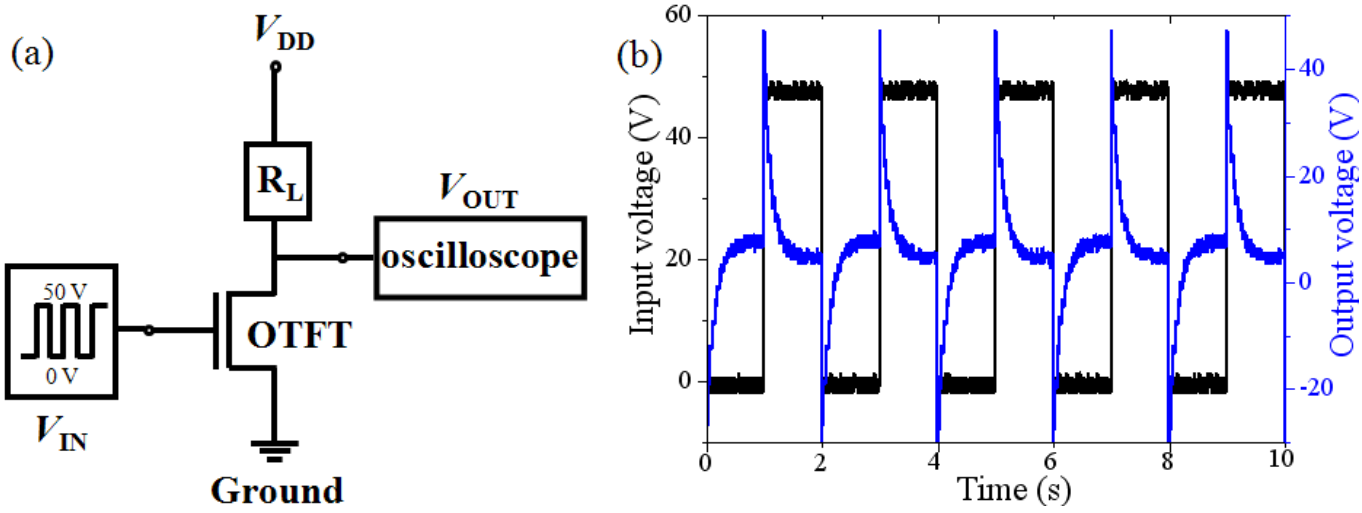

Figure 6

Table 1. Summary of performance of OTFTs with **3b**

Gate dielectric	Substrate Temp. (^{o}C)	Mobility (cm^2/Vs)	I_{on}/I_{off} ratio	V_{th} (V)	S.S (V/dec)
Bare SiO_2	25	6.2×10^{-4}	3.8×10^{3}	44.8	2.4
Bare SiO_2	45	5.5×10^{-4}	7.5×10^{1}	70.7	2.5
Bare SiO_2	60	5.9×10^{-6}	1.6×10^{1}	50.0	13.9
OTS-SiO_2	25	1.2×10^{-2}	1.2×10^{5}	51.0	1.3
OTS-SiO_2	45	1.7×10^{-2}	3.1×10^{4}	48.2	2.1
OTS-SiO_2	60	3.8×10^{-3}	2.5×10^{4}	50.1	3.4
CL-PVP*	25	3.6×10^{-4}	5.8×10^{2}	26.7	5.6
CL-PVP*	45	1.9×10^{-4}	3.4×10^{3}	26.5	5.6
CL-PVP*	60	7.6×10^{-5}	1.2×10^{2}	28.5	15.4

*CL-PVP: Cross-linked poly(4-vinylphenol)